

Stable local moments of vacancies and hollow-site impurities in graphene

M. Mashkooi¹ and S. A. Jafari^{1,2,3}

¹Department of Physics, Sharif University of Technology, Tehran 11155-9161, Iran

²Center of excellence for Complex Systems and Condensed Matter (CSCM),
Sharif University of Technology, Tehran 145889694, Iran

³School of Physics, Institute for Research in Fundamental Sciences (IPM), Tehran 19395-5531, Iran

Taking into account the possibility of a p-wave hybridization function $V(\vec{k})$ of ad-atom with Dirac electrons in graphene – which arises for vacancies and hollow-site impurities – we study the nature of magnetic moment formation within the single impurity Anderson model (SIAM). Compared to the s-wave hybridization function, we find that the local moments formed within the Hartree mean field are robust against the change in the parameters of the model. Further we investigate the stability of the local moments with respect to quantum fluctuations by going beyond the Hartree approximation. We find that for parameter regimes where local moments formed by top-site ad-atoms are completely washed out by quantum fluctuations, those formed by vacancies (or hollow-site impurities) survive the quantum fluctuations captured by post-Hartree approximation. Hence vacancies and hollow-site ad-atoms are suitable candidates to produce stable local moments.

PACS numbers: 45.20.Hr, 73.22.Pr, 81.05.ue

I. INTRODUCTION

Since its isolation in the laboratory, graphene has stimulated extensive research activity among condensed matter and material physicists^{1–3}. Distinct features of graphene are its two dimensional structure and the nature of low-energy excitations which are described by the Dirac equation⁴. These two characteristics lead to fascinating properties of graphene. For example two dimensionality allows for tuning the carrier type density via a gate voltage as well as the possibility of adding/substituting various atoms on graphene⁵. The two dimensional structure further allows to conveniently remove some of the carbon atom to create vacancies which are responsible for spin-half magnetic states⁶. The potential distortion resulting from the creation of a vacancy can in turn lead to a shallow impurity state which can hybridize with $2p_z$ orbitals of three neighboring carbon atoms. Assumption of such a hybridization, after Fourier transformation from localized Wannier states to corresponding Bloch wave-functions results in a momentum dependence in the hybridization matrix element $V(\vec{k})$ between the state localized on vacancy and the π -bands of graphene, which after linearization around the Dirac points acquires at low-energies the functional form of a p-wave dependence on momentum^{7,8}:

$$V(\vec{k}) = (k_x - ik_y)\tilde{V} \quad (1)$$

The above form is consistent with the fact that the pseudo-spin structure of the Bloch wave functions in graphene allows them to hybridize with external states in both $l = 0$ and $l = 1$ angular momentum channels⁹. The above form also holds for the hybridization between the localized states of an ad-atom in a hollow-site position which hybridizes with *both* sublattices via $V(\vec{k})$ and $V^*(\vec{k})$ functional forms. In this respect hollow-site ad-atoms and vacancies differ from top-site impurities in that they have p-wave hybridization, while the later has s-wave hybridization.

The phase diagram of magnetic states in graphene has been previously studied by Uchoa and coworkers¹⁰. They studied

the $l = 0$ channel⁹ corresponding to momentum-independent hybridization function. Within the Hartree mean field theory they obtained a phase diagram for the magnetic states which significantly differs from the corresponding one for ordinary metals¹¹. In this work we focus on the momentum dependent hybridization function of the p-wave form relevant to vacancies and hollow-site ad-atoms, and investigate the local spectral properties of the SIAM both within and beyond the Hartree mean field. Within the mean field, in contrast to the momentum-independent case¹⁰, we find that magnetic states are formed in much larger region of the parameter space. This could be interpreted as the parametric robustness of the local moments arising from vacancies or hollow-site ad-atoms. Then within the equation of motion approach we proceed one step beyond the Hartree decoupling and find that the local moments due to p-wave hybridization display stability against quantum fluctuations beyond the mean field theory. These findings shed light on the experimentally observed formation of spin-half states which are attributed to vacancies in graphene⁶.

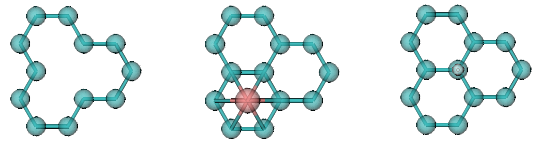


FIG. 1: Vacancy (left), hollow site ad-atom (middle) and top-site ad-atoms (right) in graphene. The impurity state centered around the vacancy hybridizes with three carbon atoms form a sublattice, while the hollow site ad-atom in addition hybridizes with another three atoms from the other sublattice. The impurity orbital associated with the top-site impurity hybridizes only with the $2p_z$ orbital of one underneath carbon atom.

II. FORMULATION OF THE PROBLEM

The Anderson model for graphene with a vacancy can be written as,

$$H = H_g + H_{\text{hyb}} + H_{\text{imp}}$$

The first term of above Hamiltonian describes π electrons of graphene. The second term describes hybridization of impurity state with Dirac fermions in graphene. To create a vacancy we assume that a carbon atom from A-sublattice has been removed. These terms after a standard Hartree mean field factorization will be written as

$$\begin{aligned} H_g &= -t \sum_{\vec{k}\sigma} (\phi(\vec{k}) a_{\vec{k}\sigma}^\dagger b_{\vec{k}\sigma} + \phi^*(\vec{k}) b_{\vec{k}\sigma}^\dagger a_{\vec{k}\sigma}) \\ H_{\text{hyb}} &= \frac{1}{\sqrt{N}} \sum_{\vec{k}\sigma} V(\vec{k}) b_{\vec{k}\sigma}^\dagger d_\sigma + h.c. \\ H_{\text{imp}} &= \sum_{\sigma} \varepsilon_\sigma d_\sigma^\dagger d_\sigma \quad ; \varepsilon_\sigma \equiv \varepsilon_0 + U \langle n_{\bar{\sigma}} \rangle \end{aligned} \quad (2)$$

where $\phi(\vec{k}) = \sum_{n=1}^3 \exp(-i\vec{\delta}_n \cdot \vec{k})$ is the form factor associated with three neighbors connected by vectors $\vec{\delta}_n$, with $n = 1, 2, 3$. The creation operators $a_{\vec{k}\sigma}^\dagger$ and $b_{\vec{k}\sigma}^\dagger$ create Bloch electrons on A and B sublattices with spin σ , respectively and d_σ^\dagger creates an electron with spin σ in the impurity state associated with the vacancy. Here ε_0 is the impurity level, which after incorporating the Hubbard repulsion U splits into two sub-levels denoted by ε_σ . The hybridization function $V(\vec{k})$ as emphasized in Eq. (1) is proportional to the form factor $\phi(\vec{k})$ which in the continuum limit becomes proportional $k_x - ik_y$.

After the Hartree mean field factorization implicit in Eq. (2), the impurity Green function can be written as,

$$G_{d\sigma}^{-1}(\omega) = \omega - \varepsilon_\sigma - \Sigma_d^\Delta(\omega) \quad (3)$$

where,

$$\Sigma_d^\Delta(\omega) = \sum_{\vec{k}} |V(\vec{k})|^2 \frac{\omega}{\omega^2 - t^2 |\phi(\vec{k})|^2} \quad (4)$$

The above integral can be easily evaluated to give,

$$-\frac{\omega\Delta}{\pi t^2} \left[D^2 + \omega^2 \ln\left(\frac{|\omega^2 - D^2|}{\omega^2}\right) + i\pi\omega|\omega|\theta(D - |\omega|) \right] \quad (5)$$

where $\Delta \equiv \frac{\pi V^2}{D^2}$, where $D \sim 7\text{eV}$ is the high-energy band cutoff chosen such that the total number of electrons in the linearized band are the same as π -band. Note that in contrast to the momentum-independent case – see. Eq. (22) – where the imaginary part of the Σ_d^Δ is proportional $|\omega|$, here the p-wave momentum-dependence of the hybridization gives rise to anomalous $|\omega|^3$ dependence in the imaginary part of Σ_d^Δ . Inserting the above equation in (3) the impurity Green function becomes,

$$G_{d\sigma}(\omega) = \frac{1}{Z^{-1}(\omega)\omega - \varepsilon_\sigma + i|\omega|^3\Delta\theta(D - |\omega|)/t^2}, \quad (6)$$

where $Z^{-1}(\omega)$ is given by,

$$Z^{-1}(\omega) = 1 + \frac{V^2}{t^2 D^2} [D^2 + \omega^2 \ln(|\omega^2 - D^2|/\omega^2)]. \quad (7)$$

The imaginary part of $\Sigma_d^\Delta(\omega)$ shows the broadening of localized level due to hybridization. Here, in contrast to normal metals, the broadening displays strong ω -dependence. The ω -dependence in the p-wave case is even stronger than the s-wave case. Then the local spectral function becomes,

$$A_{d\sigma}(\omega) = \frac{\Delta}{\pi t^2} \frac{|\omega|^3 \theta(D - |\omega|)}{(Z^{-1}(\omega)\omega - \varepsilon_\sigma)^2 + \Delta^2 \omega^6 / t^4} \quad (8)$$

which in turn gives the occupation of σ sub-band as,

$$n_\sigma = \frac{\Delta}{\pi t^2} \int_{-\infty}^{\mu} d\omega \frac{|\omega|^3 \theta(D - |\omega|)}{(Z^{-1}(\omega)\omega - \varepsilon_\sigma)^2 + \Delta^2 \omega^6 / t^4} \quad (9)$$

In this equation, the n_\uparrow is given as an integral involving ε_\uparrow which itself depends on n_\downarrow as given by Eq. (2). These equations for n_\uparrow and n_\downarrow must be solved self-consistently. Eq. (8) must be compared to Eq. (9) of Ref.¹⁰ corresponding to s-wave hybridization of top-site impurities. In order to make the comparison, we have introduced function $Z^{-1}(\omega)$ along with the notations of this reference. The function $Z^{-1}(\omega)$ in our case differs from the \vec{k} -independent hybridization in two respects: (i) the logarithmic part of the ω -dependence has acquired an anomalous ω^2 factor compared to \vec{k} -independent case. (ii) Comparing Σ_d^Δ of the s-wave case – Eq. (22) – in the p-wave case an additive D^2 term appears. To complete the self-consistency cycle, one needs to accurately evaluate the integrals connecting n_\uparrow and n_\downarrow . The authors of Ref.¹⁰ argue that, neglecting the ω -dependence of $Z^{-1}(\omega)$ allows for analytic evaluation of the integral at the cost of introducing a few percent error. But as we will show in the sequel, since such errors are repeated several times through out the self-consistency cycle, the final result are sensitive to the ω -dependence of the $Z^{-1}(\omega)$ function.

III. NUMERICAL RESULTS

In this section we present numerical results for the self-consistent solution at the level of Hartree mean field equations. To begin with, we revisit the top-site hybridization case discussed in Ref.¹⁰ and show how the approximation of neglecting the ω -dependence of $Z^{-1}(\omega)$ leads to qualitatively different phase diagram. Then we focus on the case of p-wave hybridization function pertinent to vacancy and hollow-site impurities.

A. Local moments from top-site impurities

In this case the hybridization $V_{\vec{k}}$ does not depend on \vec{k} , and the occupation of spin σ impurity sub-band is given by¹⁰,

$$n_\sigma = -\frac{1}{\pi} \int_{-D}^{\mu} d\omega \frac{\Delta |\omega| \theta(D - |\omega|)}{[Z^{-1}(\omega)\omega - \varepsilon_\sigma]^2 + \Delta^2 \omega^2}, \quad (10)$$

where

$$Z^{-1}(\omega) = 1 + \frac{V^2}{D^2} \ln\left(\frac{|D^2 - \omega^2|}{\omega^2}\right). \quad (11)$$

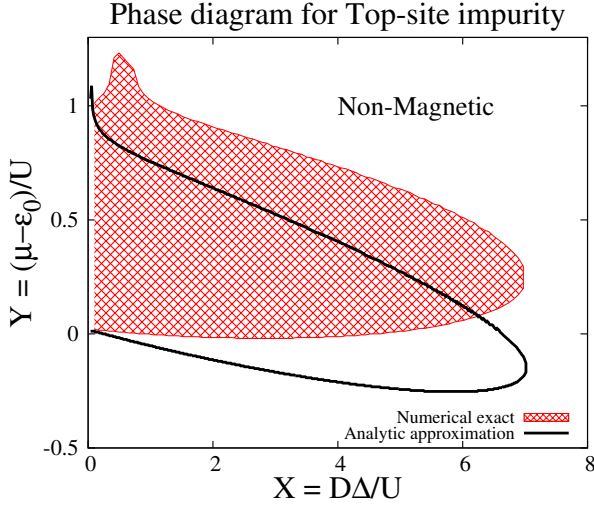


FIG. 2: (Color online) Phase diagram for the local moment formation in SIAM for top-site impurity in graphene. The area enclosed by the curves and the Y -axis is magnetic. In this plot the variables X and Y are defined by $X = \frac{D\Delta}{U}$, $Y = \frac{(\mu - \varepsilon_0)}{U}$. Other parameters are $\frac{V}{D} = 0.14$ and $\frac{\varepsilon_0}{D} = 0.043$. The black thick solid line corresponds to the approximate analytic integration of Ref.¹⁰. The red (filled) plot corresponds to numerically exact evaluation of integrals.

Here we do not apply the approximation $Z^{-1}(\omega) \approx Z^{-1}(\varepsilon_\sigma)$ and retain the full energy dependence of Z^{-1} . The price one has to pay is to do the integrations necessary to get n_σ numerically. We define two standard variables $X = D\Delta/U$ and $Y = (\mu - \varepsilon_0)/U$ in terms of which the phase diagram is traditionally constructed¹¹. The result is shown in Fig. 2. The black (thick solid) plot corresponds to the approximate solution where the energy dependence of Z^{-1} has been neglected. In the red plot (filled plot) retaining the full energy dependence of Z^{-1} the integrals are evaluated numerically. As can be seen, there are two major differences: (i) The numeric result compared to the approximate one shows a significant shift of the lower lobe of the phase boundary to positive Y values corresponding to $\mu > \varepsilon_0$. In this respect for the top-site impurity states in graphene magnetic states are dominantly in $\mu > \varepsilon_0$ region, akin to normal metals. The asymmetry of the graph around $Y = 0.5$ however is the feature distinct from normal metals and upon precise calculation of integrals this asymmetry will be even more enhanced for the same set of parameters indicated in the figure caption. (ii) The second qualitative difference is that the re-entrant behavior seen as a hump for small values of X will be more pronounced when the integrals are evaluated exactly. Although neglecting the energy dependence in Z^{-1} leads only to small error in each evaluation of the integral, repeating this procedure in the self-consistency process, propagates and enhances the errors. With this point in mind, in the following we avoid using such approximations and focus on the self-consistent solution of the mean field equations for the p-wave hybridization function.

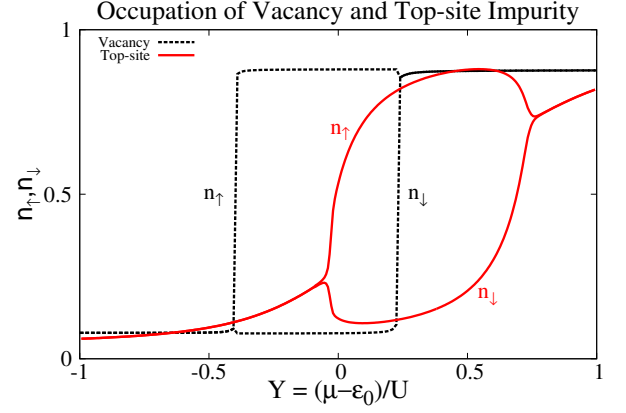


FIG. 3: (Color online) Comparison of the self-consistent mean field occupations n_\uparrow and n_\downarrow as a function of Y for a fixed value $X = 5.0$ for the vacancy (black dashed line) and top-site impurity (red solid line). The region of local moment formation for vacant graphene is shifted towards negative values of Y in comparison to top-site case. Moreover within the whole region, magnetic moment formed via p-wave hybridization is more or less constant and suddenly drops to zero at the phase boundary, while in the case of top-site impurity, the moment smoothly vanishes by approaching the boundary.

B. Local moments from vacancies or hollow-site impurities

Now we proceed by self-consistently solving the mean field equations (8) for vacancy induced local moments. In Fig. 3 we compare the self-consistently determined values of occupation numbers n_\uparrow and n_\downarrow for a fixed value of $X = 5.0$ in the two cases corresponding to top-site impurity and vacancy. For very small and very large values of Y the n_\uparrow and n_\downarrow curves coincide which means the magnetic moment is zero. For intermediate values of Y the curves corresponding to n_\uparrow and n_\downarrow split. The amount of splitting determines the magnetic moment. As can be seen the local moment formation region in vacancy sets in smaller values of Y on the negative values, while in the top-site case, the local moment region sets in $\mu - \varepsilon_0 \lesssim 0$. Moreover in the case of vacancy the magnetic moment inside the local moment region stays more or less constant and abruptly vanishes by approaching the boundary, while in the top-site case, the local moment smoothly vanishes as the boundary is reached.

Repeating the above analysis for other values of X we obtain the phase diagram depicted in Fig. 4. This plot has been generated for $V/D = 0.14$ and two different values of $\varepsilon_0/D = 0.029$ and $\varepsilon_0/D = 0.043$ as indicated in the figure. The plots corresponding to $\varepsilon_0/D = 0.043$ in this figure can be compared to the one in Fig. 2 of the top-site impurities as they correspond to the same set of parameters. As can be noted by comparing Fig. 2 and Fig. 4, in the case of p-wave hybridization, the local magnetic moments are found in a much larger region of parameter space. This can be interpreted as the parametric robustness of local moments arising from vacancies or hollow-site impurity states compared to those due to top-site impurity states. Another important aspect can be noticed by comparison of the p-wave phase diagram to the numerically

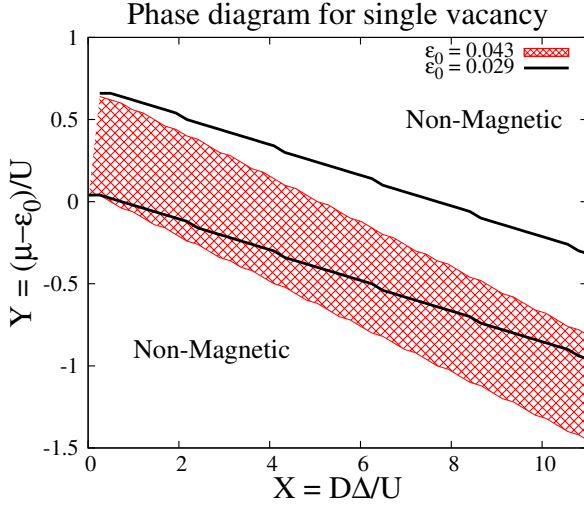


FIG. 4: (Color online) Local moment phase diagram of the single vacancy Anderson model. The variables X and Y are defined by $X = \frac{\Delta D}{U}$, $Y = \frac{(\mu - \varepsilon_0)}{U}$. The parameters in both plots are $\frac{V}{D} = 0.14$ while their impurity energy levels are different, with filled (red) plot corresponding to $\frac{\varepsilon_0}{D} = 0.043$ and thick solid (black) line corresponding to $\frac{\varepsilon_0}{D} = 0.029$.

exact plot in Fig. 2 of s-wave case is that in the later case the local moment region dominantly lies in the positive values of Y , a feature also shared by normal metals, while in the former case, the local moment region is substantially extended to negative values of Y and has been elongated as an stripe shaped region. Such elongation has been reported in a similar study for bilayer graphene¹² and has been shown to arise from a large contribution in the real part of the self-energy in the vacant case which arises from a constant shift on the scale of bandwidth D . Such self-energy shifts can be absorbed into ε_0 defining a largely shifted effective $\tilde{\varepsilon}_0$. This is consistent with the fact that small changes in ε_0 does not change the elongated nature of the phase diagram. Moreover up to quite large values of $X \sim 12$ – which is already much larger than physically conceivable values for physical graphene – the width of the range of Y values for which the local moment is formed does not vary much. The larger magnetic moment formation area in the phase space can be interpreted as the robustness of the local moments formed by vacancies compared to top-site impurities, and is consistent with the observed spin-half magnetic moment in vacant graphene⁶.

C. Internal structure of the impurity orbital in hollow-site ad-atoms

Large ad-atoms prefer the hollow-site position when added to a graphene sheet¹³ while small atoms such as hydrogen prefer the top-site position⁵. Therefore implicit assumption of s-wave orbital structure for the impurity atom itself is only feasible for top-site positions. With larger ad-atoms in the hollow-site positions, higher multiplicities and more complex symmetry patterns may appear. In this section we address

the question local moment formation for impurity orbitals that preserve the time reversal symmetry within the Hartree mean field theory. For the case of hollow-site ad-atom, the s-wave symmetry is formally identical to what we considered in the vacancy case and that is why we treated these two cases on the same footing. The only difference between them is that the Σ_d^Δ in the s-wave hollow-site case is twice the vacancy case. The reason is simply related to the fact that now in addition to three nearest neighbors from a given sublattice, three nearest neighbors from the other sublattice also emerge. Hence the phase diagram of local moments in the case of s-wave ad-atom in the hollow-site position is identical to that of vacancy after a re-scaling of hybridization strength V , i.e.: $V^{\text{hollow-site}} = \sqrt{2}V^{\text{vacancy}}$.

The p orbitals alone can not form a linear combination compatible with the six-fold rotational symmetry of graphene. The linear combination of d orbitals compatible with the symmetries of honeycomb hexagon requires complex coefficients which breaks the time reversal symmetry. Therefore the simplest non-trivial higher angular momentum pattern compatible with the rotational symmetry of the honeycomb lattice is the f -wave pattern. For this purpose we consider in the hollow-site configuration a hybridization Hamiltonian of the following form,

$$H_{\text{hyb}} = \frac{V}{\sqrt{N}} \sum_{\vec{k}\sigma} (\phi(\vec{k})b_{\vec{k}\sigma}^\dagger + e^{i\alpha}\phi^*(\vec{k})a_{\vec{k}\sigma}^\dagger)d_\sigma + h.c. \quad (12)$$

In above Hamiltonian, when the parameter α takes the value π it corresponds to f -wave pattern of the atomic orbital. Obviously $\alpha = 0$ reduces to the s-wave atomic orbital where the impurity is hybridized with both A and B sublattice equivalently, while in f -wave case the hybridization pattern changes the sign of V after each $2\pi/6$ rotation.

The equation of motion for the Green function of the above Hamiltonian will now depend on the phase α ,

$$G_{d\sigma}^{-1}(\omega) = \omega - \varepsilon_0 - \Sigma_d^\Delta(\omega) \quad (13)$$

where the dependence on α is through the self energy:

$$\Sigma_d^\Delta(\omega) = V^2 \sum_{\vec{k}} \frac{\omega}{\omega^2 - t^2 |\phi(\vec{k})|^2} (g(\vec{k}, \omega) + e^{-2i\alpha} g^*(\vec{k}, \omega)),$$

$$g^*(\vec{k}, \omega) \equiv \frac{v_F^2 k^2}{t^2} (1 - v_F k e^{i(3\theta + \alpha)}) / \omega. \quad (14)$$

For both α values of zero and π , we have $e^{-2i\alpha} = 1$. Furthermore the θ integration of $e^{i(3\theta + \alpha)}$ produces zero. Therefore the self energy at the Hartree level will not depend on α , and the difference between s-wave and f -wave internal structures of the impurity orbital does not appear at the mean field level.

IV. STABILITY OF MEAN-FIELD APPROXIMATION

So far we have investigated within the mean field level the formation of local moments for two situations corresponding to the s-wave and p-wave hybridization function $V(\vec{k})$. We have further checked that in the hollow site case the internal

structure of the impurity orbital itself does not matter within the mean field theory. When the local moments are formed in the Hartree mean field level, the question will be, what happens to the local magnetic moments when quantum fluctuations beyond the mean field are taken into account. A proper treatment of the effect of fluctuations leads to the dynamical screening of the magnetic moment (Kondo screening). In this section we address this question by going one step beyond the Hartree mean field within the equation of motion approach. To do this we use the standard notation for the Fermionic correlation functions:

$$\langle\langle f_\sigma(t) | f_\sigma^\dagger(t') \rangle\rangle = -i\theta(t-t')\langle\{f_\sigma(t) | f_\sigma^\dagger(t')\}\rangle. \quad (15)$$

Writing the equation of motion for the above Green function in frequency domain gives,

$$(\omega - \varepsilon_0 - \Sigma_d^\Delta(\omega))\langle\langle f_\sigma | f_\sigma^\dagger \rangle\rangle = 1 + U\langle\langle f_\sigma n_{\bar{\sigma}} | f_\sigma^\dagger \rangle\rangle. \quad (16)$$

In the Hartree approximation the correlation function on the right of Eq. (16) is approximated by $\langle n_{\bar{\sigma}} \rangle \langle\langle f_\sigma | f_\sigma^\dagger \rangle\rangle$, which closes the equations, and the effect of Hubbard U will be to replace $\varepsilon_0 \rightarrow \varepsilon_\sigma = \varepsilon_0 + U\langle n_{\bar{\sigma}} \rangle$. But here we do not close the equations at this level and proceed one step further by writing another equation of motion for correlation function $\langle\langle f_\sigma n_{\bar{\sigma}} | f_\sigma^\dagger \rangle\rangle$. This gives,

$$\omega\langle\langle f_\sigma n_{\bar{\sigma}} | f_\sigma^\dagger \rangle\rangle = \langle\{f_\sigma n_{\bar{\sigma}}, f_\sigma^\dagger\}\rangle + \langle\langle [f_\sigma n_{\bar{\sigma}}, H] | f_\sigma^\dagger \rangle\rangle. \quad (17)$$

Let us first focus on the simplest case which is the top-site case. In this case, calculation of the (anti) commutation relations needed in the above equation we find:

$$(\omega - \varepsilon_0 - U)\langle\langle f_\sigma n_{\bar{\sigma}} | f_\sigma^\dagger \rangle\rangle = \langle n_{\bar{\sigma}} \rangle + V \sum_{\vec{k}} \langle\langle b_{\vec{k}\sigma}^\dagger n_{\bar{\sigma}} + f_\sigma (f_{\bar{\sigma}}^\dagger b_{p\bar{\sigma}} - b_{p\bar{\sigma}}^\dagger f_{\bar{\sigma}}) | f_\sigma^\dagger \rangle\rangle. \quad (18)$$

At this stage the decoupling scheme can be applied to the correlation function on the right hand side of Eq. (18) as follows:

$$\langle\langle b_{\vec{k}\sigma}^\dagger n_{\bar{\sigma}} + f_\sigma (f_{\bar{\sigma}}^\dagger b_{p\bar{\sigma}} - b_{p\bar{\sigma}}^\dagger f_{\bar{\sigma}}) | f_\sigma^\dagger \rangle\rangle \approx \langle n_{\bar{\sigma}} \rangle \langle\langle b_{\vec{k}\sigma}^\dagger | f_\sigma^\dagger \rangle\rangle + \langle\langle f_{\bar{\sigma}}^\dagger b_{p\bar{\sigma}} - b_{p\bar{\sigma}}^\dagger f_{\bar{\sigma}} | f_\sigma^\dagger \rangle\rangle \langle\langle f_\sigma | f_\sigma^\dagger \rangle\rangle \quad (19)$$

The above decoupling has been performed in such a way to avoid off-diagonal correlation functions in the spin-indices. Hence the operators carrying $\bar{\sigma}$ spin index are taken out of the correlations in the form of expectation values¹⁴. Finally to close the set of equations of motion, we write the equation of motion for $\langle\langle b_{\vec{k}\sigma}^\dagger | f_\sigma^\dagger \rangle\rangle$, which gives,

$$\langle\langle b_{p\sigma} | f_\sigma^\dagger \rangle\rangle = V \frac{\omega}{\omega^2 - t^2 |\phi(\vec{k})|^2} \langle\langle f_\sigma | f_\sigma^\dagger \rangle\rangle. \quad (20)$$

Therefore at the present approximation, the local Green function becomes,

$$\langle\langle f_\sigma | f_\sigma^\dagger \rangle\rangle = [\omega - \varepsilon_0 - \Sigma_d^\Delta(\omega) - \Sigma'(\omega)]^{-1}, \quad (21)$$

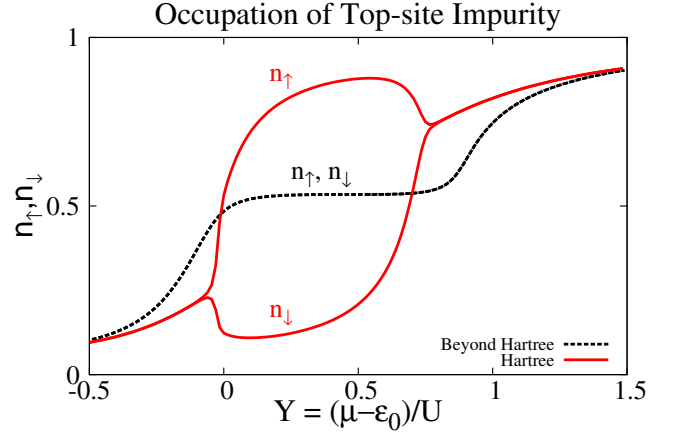


FIG. 5: (Color online) The self-consistent occupations n_\uparrow and n_\downarrow for top site impurity as a function of Y for a fixed value $X = 5.0$ and $\varepsilon_0 = 0.029$. As indicated in the legend, within the Hartree approximation (solid red line), the n_\uparrow and n_\downarrow plots are split, which indicates the formation of local moments at Hartree level. But as soon as we go beyond the Hartree approximation (dashed black line), for the same values of parameters, the n_\uparrow and n_\downarrow curves collapse on each other. This means that fluctuations beyond the Hartree approximation destroy the local moments formed at the mean field level.

where Σ_d^Δ describe the hybridization of local electrons with the band continuum and for the top site situation is given by¹⁰

$$\Sigma_d^\Delta(\omega) = -V^2 \frac{\omega}{D^2} \ln \left(\frac{|\omega^2 - D^2|}{\omega^2} \right) - iV^2 \frac{\pi|\omega|}{D^2} \theta(D - |\omega|). \quad (22)$$

In the p-wave case as is shown in the appendix, within the present approximation, the form of the local Green function remains the same as Eq. (21). The only difference is that now the hybridization function Σ_d^Δ for hollow site case is given by Eq. (5). Since the Hubbard U acts only locally in the impurity orbital, at this level of approximation, the self-energy correction coming from the hybridization, Σ_d^Δ , and those coming from Hubbard term, Σ' , are separable and hence the later turns out to be insensitive to the nature of hybridization of the impurity orbital with neighboring orbitals. The interaction effects arising from the Hubbard U are given by the self-energy $\Sigma'(\omega)$ as follows:

$$\Sigma'(\omega) \equiv \frac{U(\omega - \varepsilon_0)\langle n_{\bar{\sigma}} \rangle}{\omega - \varepsilon_0 - U(1 - \langle n_{\bar{\sigma}} \rangle)}. \quad (23)$$

Note that in this case, unlike the Hartree approximation where the mere effect of Hubbard U is to shift ε_0 by $U\langle n_{\bar{\sigma}} \rangle$, in the present approximation, the self-energy not only is not of a simple shift form, but also has acquired a non-trivial ω -dependence.

In Fig. 5 we have compared the self-consistent solutions for the occupation of the \uparrow and \downarrow spin sub-bands within the Hartree and our post-Hartree approximation for the top-site impurity. The plot has been generated for a fixed value of $X = 5.0$ and $\varepsilon_0 = 0.029$ as function of Y . Within the Hartree approximation plots corresponding to n_\uparrow and n_\downarrow are split for

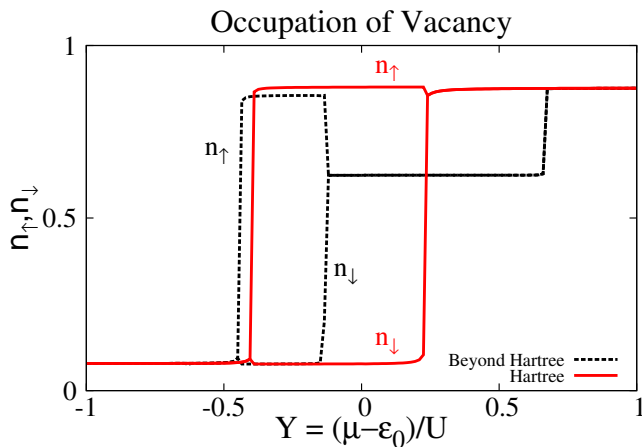


FIG. 6: (Color online) The self-consistent occupations n_{\uparrow} and n_{\downarrow} for hollow site impurity as a function of Y for a fixed value $X = 5.0$ and $\varepsilon_0 = 0.029$. The region of local moment formation is where the n_{\uparrow} and n_{\downarrow} curves split apart. The solid line (red) corresponds to Hartree approximation, and the dashed lines (black) correspond to post-Hartree approximation. In the p-wave hybridization case as can be seen by including the self-energy Eq. (23), the local moment region is shrunk, but it does not vanish. In this sense, local moments formed by hollow-site impurities are robust against quantum fluctuations.

positive values of Y . This indicates the formation of local moments at the Hartree level. However as soon as we employ the self-energy (23) to go beyond the Hartree, the n_{\uparrow} and n_{\downarrow} plots collapse on each other. Therefore the local moments formed at the Hartree level are destroyed by quantum fluctuations beyond the mean field level.

In Fig. 6 we plot the same set of data as in Fig. 5 but for the p-wave hybridization function. The interesting feature to note in this case is that, even by including the self-energy effect Eq. (23) which goes an step beyond the Hartree approximation, still there will be a region in the parameter space where the local moment survives the fluctuations. Therefore the local moments formed by hollow-site impurities (or vacancies) when compared to those due to top-site impurities, not only are more robust in terms of the extension of region in the parameter space where local moment is formed, but they are also robust against the quantum fluctuation effects captured by Eq. (23). This makes vacancies and hollow-site impurity states ideal sources of local magnetic moments in graphene which are hard to destroy. This can account for the observed magnetic moments in vacant graphene⁶.

V. SUMMARY AND DISCUSSION

In this paper we investigated the formation of local moments in a graphene sheet, in two situations corresponding to s-wave and p-wave functional dependence in the hybridization function $V(\vec{k})$ within the single impurity Anderson model. The former corresponds to the top-site impurities, while the later may correspond to hollow-site impurities or vacancies. First we noted that the output of the self-consistency cycle is very sensitive to the precision of the integrations. Any approximation in the integrations propagates the errors thorough the self-consistency cycle and may give rise to different results. Then we compared the Hartree mean field level phase diagram of the above two cases. We found that vacancies and hollow-site impurities give rise to much larger region in the phase space where the magnetic moments are formed. In this sense the local moments arising from impurity's orbitals on the hollow-sites or from vacancies are robust against change in the parameters. Further we showed that within the Hartree mean field the internal structure of the impurity orbital itself does not affect the local moment properties. Then within the equation of motion method, we proceeded one step beyond Hartree approximation and derived a self-energy due to Hubbard U term which takes into account quantum fluctuations beyond the Hartree mean field. Within such a post-Hartree mean field we obtained the self-consistently determined occupation numbers of the \uparrow and \downarrow spin impurity sub-bands. We found that in the top-site case, the quantum fluctuations in the post-Hartree approximation can destroy the local moments formed at Hartree level, while in the case of vacancies and hollow-site impurities, for the same set of parameters, the local moments survive the quantum fluctuations within our approximation. Therefore we conclude that the p-wave hybridization functions gives rise to local moments which are not only robust in parameter space, but are also immune to quantum fluctuations beyond the Hartree mean field. The present stability analysis is consistent with the observed spin-half magnetic states in vacant graphene⁶.

VI. ACKNOWLEDGEMENT

We thank T. Tohyama for useful discussions. This research was completed while the SAJ was visiting Yukawa Institute for Theoretical Physics by the fellowship S13135 from Japan Society for Promotion of Science.

¹ K. S. Novoselov, A. K. Geim, S. V. Morozov, D. Jiang, Y. Zhang, S. V. Dubonos, I. V. Grigorieva, and A. A. Firsov, *Science* **306**, 666 (2004).

² K. S. Novoselov, A. K. Geim, S. V. Morozov, D. Jiang, M. I. Katsnelson, I. V. Grigorieva, S. V. Dubonos, and A. A. Firsov, *Nature* **438**, 197 (2005).

³ Y. Zhang, Y. W. Tan, H. L. Stormer, and P. Kim, *Nature* **438**, 201

(2005).

⁴ A. H. Castro Neto, F. Guinea, N. M. R. Peres, K. S. Novoselov, and A. K. Geim, *Rev. Mod. Phys.* **81**, 109 (2009).

⁵ D. Haberer, C. E. Guisica, Y. Wang, H. Sachdev, A. V. Fedorov, M. Farjam, S. A. Jafari, D. V. Vyalikh, D. Usachov, X. Liu, U. Treske, M. Grobosch, O. Vilkov, V. K. Adamchuk, S. Irle, S. R. P. Silva, M. Knupfer, B. Büchner, and A. Grüneis, *Adv. Mater.* **23**,

- 4487 (2011).
- ⁶ R. R. Nair, M. Sepioni, I. L. Tsai, O. Lehtinen, J. Keinonen, A. V. Krasheninnikov, T. Thomson, A. K. Geim, and I. V. Grigorieva Nat. Phys. **8**, 199 (2012).
- ⁷ B. Uchoa, T. G. Rappoport, and A. H. Castro Neto, Phys. Rev. Lett. **106**, 016801 (2011).
- ⁸ S. A. Jafari, T. Tohyama, arXiv:1308.4173 (2013).
- ⁹ K. Sengupta, G. Baskaran, Phys. Rev. B **77**, 045417 (2008).
- ¹⁰ B. Uchoa, V. N. Koto, N. M. R. Peres, and A. H. Castro Neto, Phys. Rev. Lett. **101**, 026805 (2008).
- ¹¹ P. W. Anderson, Phys. Rev. **124**, 41 (1961).
- ¹² M. Killi, D. Heidarian, A. Paramekanti, New J. Phys. **13**, 053043 (2011).
- ¹³ K. T. Chan, J. B. Neaton, M. L. Cohen, Phys. Rev. B. **77**, 235430 (2008).
- ¹⁴ J. Hubbard, Proc. R. Soc. Lond. A **276**, 238 (1963).

Appendix A: Beyond Hartree: hollow-site case

In this appendix we calculate the impurity Green function one step beyond the Hartree mean-field approximation for hollow-site impurity. The equation of motion for local Green function is given by Eq. (16). Avoiding the decoupling of $\langle\langle n_{\bar{\sigma}} f_{\sigma} | f_{\sigma}^{\dagger} \rangle\rangle$ and writing an equation of motion for it we obtain,

$$\omega \langle\langle f_{\sigma} n_{\bar{\sigma}} | f_{\sigma}^{\dagger} \rangle\rangle = \langle n_{\bar{\sigma}} \rangle + \langle\langle [f_{\sigma} n_{\bar{\sigma}}, H] | f_{\sigma}^{\dagger} \rangle\rangle, \quad (\text{A1})$$

which after evaluation of the necessary commutation relations becomes,

$$(\omega - \varepsilon_0 - U) \langle\langle f_{\sigma} n_{\bar{\sigma}} | f_{\sigma}^{\dagger} \rangle\rangle = \langle n_{\bar{\sigma}} \rangle + V \sum_{\vec{k}} \langle\langle c_{\vec{k}\sigma} n_{\bar{\sigma}} + f_{\sigma} (f_{\bar{\sigma}}^{\dagger} c_{\vec{k}\bar{\sigma}} - c_{\vec{k}\bar{\sigma}}^{\dagger} f_{\bar{\sigma}}) | f_{\sigma}^{\dagger} \rangle\rangle. \quad (\text{A2})$$

In above equation the operator $c_{\vec{k}\sigma}^{\dagger}$ is defined by

$$c_{\vec{k}\sigma}^{\dagger} \equiv \phi(\vec{k}) b_{\vec{k}\sigma}^{\dagger} + \phi^*(\vec{k}) a_{\vec{k}\sigma}^{\dagger}. \quad (\text{A3})$$

In the hollow site configuration the impurity hybridizes with carbon atoms from both sublattices. Therefore the operator $c_{\vec{k}\sigma}^{\dagger}$ in Eq. (A2) plays the same role as $b_{\vec{k}\sigma}^{\dagger}$ in Eq. (18). We apply the same decoupling scheme which gives,

$$\begin{aligned} \langle\langle c_{\vec{k}\sigma} n_{\bar{\sigma}} + f_{\sigma} (f_{\bar{\sigma}}^{\dagger} c_{\vec{k}\bar{\sigma}} - c_{\vec{k}\bar{\sigma}}^{\dagger} f_{\bar{\sigma}}) | f_{\sigma}^{\dagger} \rangle\rangle &\approx \\ \langle n_{\bar{\sigma}} \rangle \langle\langle c_{\vec{k}\sigma} | f_{\sigma}^{\dagger} \rangle\rangle + \langle f_{\bar{\sigma}}^{\dagger} c_{\vec{k}\bar{\sigma}} - c_{\vec{k}\bar{\sigma}}^{\dagger} f_{\bar{\sigma}} \rangle \langle\langle f_{\sigma} | f_{\sigma}^{\dagger} \rangle\rangle. \end{aligned} \quad (\text{A4})$$

Hence the Green function at this approximation for hollow-site configuration will be,

$$\langle\langle f_{\sigma} | f_{\sigma}^{\dagger} \rangle\rangle = [\omega - \varepsilon_0 - \Sigma_d^{\Delta}(\omega) - \Sigma'(\omega)]^{-1}. \quad (\text{A5})$$

In the above equation the correlation effect has been encoded in self energy Σ' which in both p-wave and s-wave cases is given by Eq. (23). The only difference between the two possible hybridization functions appears in Σ_d^{Δ} which for the s-wave case is given by Eq. (22), while in the p-wave case it is given by Eq. (5).